Article

Activated-Carbon-Doped Non-Solvent-Induced Phase-Inversion Membranes: A Comprehensive Study on Synthesis, Characterisation, and Performance Evaluation

Raúl Mompó-Curell [1,*], Simbarashe Biti [2], Alicia Iborra-Clar [1,3], María Isabel Iborra-Clar [1,3], Esperanza M. Garcia-Castello [3,4] and Claudia Fernández-Martín [2,5]

1 Research Institute for Industrial Radiophysical and Environmental Safety (ISIRYM), Universitat Politècnica de València, Camino de Vera s/n, 46022 Valencia, Spain; aiborra@iqn.upv.es (A.I.-C.)

2 Chemical Processes and Materials Engineering Group, School of Engineering, University of Aberdeen, Aberdeen AB24 3UE, UK; s.biti.19@abdn.ac.uk (S.B.); cfmartin@abdn.ac.uk (C.F.-M.)

3 Department of Chemical and Nuclear Engineering, Universitat Politècnica de València, Camino de Vera s/n, 46022 Valencia, Spain; egarcia1@iqn.upv.es

4 Food Engineering Research Institute—FoodUPV, Universitat Politècnica de València, Camino de Vera, s/n. 46022 Valencia, Spain

5 Centre for Energy Transition, University of Aberdeen, Aberdeen AB24 3UE, UK

* Correspondence: raumomcu@upv.es; Tel.: +34-640191589

Abstract: Wastewater treatment often enables discharge into natural water bodies, but for effective reuse, further treatment is essential. Membrane processes provide a precise solution yet face limitations due to fouling and organic material adsorption, impacting their performance. This study focuses on synthesising ultrafiltration membranes using non-solvent-induced phase separation. These membranes are produced from a Polyethersulfone/N,N′-dimethylacetanamide (PES/DMA) solution with varying concentrations of three commercial powdered activated carbons (ACs). The membranes undergo comprehensive analysis, revealing different behaviours based on AC type and concentration in the active layer. Among the membranes, Norit R with 0.5 wt.% concentration exhibits the highest polyethylene glycol (PEG) rejection, with an impressive rejection index (R) of 80.34% and permeability coefficient of 219.29 $(L \cdot m^{-2} \cdot h^{-1} \cdot bar^{-1})$. AC-enhanced membranes display superior selectivity compared to non-doped PES membranes. This work highlights the significant influence of AC textural properties, specifically specific surface area, total micropore volume, and average micropore width, on membrane performance, particularly the rejection index.

Keywords: powder activated carbon; non-solvent-induced phase-inversion membranes; membrane characterisation; wastewater treatment; organic fouling

1. Introduction

World consumption and production are currently the engines of the economy, but consequentially, the non-controlled exploitation of natural resources has promoted destructive effects on the planet. The economic and social progress achieved during the last century has ultimately been accompanied by environmental degradation that is increasingly endangering our ecosystem.

The 2030 Agenda for Sustainable Development features Sustainable Development Goals (SDGs) consisting of several objectives for fighting climate change, preserving the environment, and optimising the design of our cities and environments. SDG number 12, "Ensure Sustainable Consumption and Production Patterns", includes among others the indication that many of the water systems that keep ecosystems thriving and feed growing human populations have been under stress. Treatment of these water systems has become fundamental to sustain their consumption and recovery [1]. Over half the world's wetlands have disappeared in the last century [2]. Agriculture consumes more water than any other

activity and wastes much of it through inefficiencies. Moreover, we can find rivers and aquifers contaminated with organic matter due to human activity that must be treated [3–5]. Accordingly, the need to preserve water systems is enormous.

Even after secondary and tertiary treatments, wastewater can only be reused with extra treatment due to organic fouling caused by humic substances, proteins, and other natural organic matter (NOM) during drinking water and wastewater treatment processes [6]. Although membrane processes can be successfully used in water recycling, they are easily fouled by organic matter. One of the frequent reasons is the accumulation and the adsorption of these materials onto the membrane surface and in the membrane pores, which may affect the membrane's performance, such as its permeability and NOM rejection [7].

Many authors have combined various types of wastewater pretreatments to reduce organic matter, such as flocculation–coagulation [8–10] and adsorption with powder AC [11] and their combinations. For example, Abdessemed et al. (2003) experimentally demonstrated that flocculation, combined with the AC adsorption process, removed 86% of the chemical oxygen demand from domestic wastewater [12]. AC is regarded as an attractive option for water treatment because it possesses a highly porous structure, large specific surface area, good chemical and physical stability, and easily adjustable textural properties and surface functionalities [13]. Additionally, due to the ability of carbon itself to bond with many other species, AC, a highly carbonaceous material, can adsorb a wide array of pollutants more effectively through various bonding mechanisms, including covalent bonding, hydrogen bonding, induced-dipole bonding, and dipole–dipole bonding [14].

In recent years, more than a thousand research articles have been published about combinations of membrane technology, mainly the bioreactor membrane, and AC adsorption. The use of AC in the membrane system was found to be very effective, not only in removing refractory organics but also in reducing membrane clogging. Nadeo et al. (2020) integrated a hybrid process (ultrasound-AC-membrane) called the USAMe® system with excellent results for the elimination of emerging compounds (up to 99%) [15]. On the other hand, Zhang et al. (2020) prepared membranes based on PES as a PES-AC-PES sandwich membrane, achieving positive results in eliminating the 17β-estradiol hormone, with a removal index of over 98% in the range of pH 2–10 [16].

Moreover, Shao et al. (2017) employed the deposition of AC on the surface of an ultrafiltration (UF) membrane. In the hybrid AC/UF process, the AC deposited on the membrane surface rarely formed a monolayer. In those cases, multilayers of AC were formed after organic matter deposition above the membrane. The AC deposition layer decreased as the size of the AC increased [17].

Liu et al. (2018) used AC and titanium dioxide (TiO_2) nanoparticles as additives to prepare polyvinylidene fluoride (PVDF) UF membranes using the phase inversion method [18]. The produced membranes can improve the hydrophilicity of their surface and its permeability, resulting in more porous membranes. The PVDF-AC membrane further exhibited excellent fouling resistance, being reduced from 40% to 25%. This study suggests that AC could be a new type of nanomaterial to develop antifouling membranes. Furthermore, UF membranes with a spherical activated carbon layer above the membrane permeate side allowed the better removal of estradiol from water [19].

In addition, some authors have prepared ultrafiltration membranes with the addition of AC, using various techniques. Ceramic membranes were prepared by Vicente et al. (2023) [20] using the centrifugal casting method. They added different concentrations of activated carbon and alumina as pore formers. The membranes obtained exhibited a considerable increase in the permeate flux, greater than 50%, but sacrificed the rejection index to the bovine serum albumin protein studied.

Finally, El-Sayed et al. (2023) fabricated membranes using the non-solvent-induced phase separation (NIPS) method, incorporating sulfonated tea wastes and activated carbon derived from sulfanilic tea wastes in a polyethersulfone matrix. The obtained membranes showed a slightly superior water flux, high rejection rates, and low fouling resistance [21].

The morphology and properties of the membrane surface, such as its charge and hydrophilic characteristics, have essential effects on the permselective properties and fouling of the membrane. These properties can be modified, especially the hydrophilic characteristic of the membrane, to reduce the electrostatic effects between the membrane charge (generally negative) and the compounds to be treated (normally positively charged). In this sense, PES is a hydrophilic polymer, and the addition of activated carbon has been considered since it is expected to increase the hydrophilic characteristic not only of the membrane surface but also of its porous structure [22].

As shown in the graphical abstract figure, hydrophilic PES membranes swell at the surface and present a more "aqueous" appearance like the surface of proteins and are repelled.

The change in surface charge is described in detail by Singh (2015) who carries out a study of different polymers and their charges and explains this phenomenon [23].

Likewise, the authors established a correlation between the molecular weight cut-off (MWCO) of PEG and the characteristic pore size of the membrane. They observed that a PES membrane with a cut-off of 20 kDa (with pore sizes around 8 nm) was obtained when the PEG employed was 30 kDa. Nevertheless, UF membranes reach up to 150 kDa MWCO, and different authors have worked with larger molecules. For instance, Lopatina et al. (2021) recently used PEG 35 kDa to characterise UF membranes [24].

The application of the UF technique combined with other techniques for treating wastewater and eliminating contaminants is well known. The authors of this study have extensive experience in this field of research. Their investigations have combined membrane techniques, ultrafiltration, and reverse osmosis after conventional physical–chemical treatment for the reuse of tannery wastewaters [25], where PES membranes with a cut-off of 30 kDa were chosen for the pre-treatment of the reverse osmosis membrane.

On the other hand, the authors belong to a research group with more than 20 years of experience in membrane manufacturing. Several research papers were published from this experience. These show that membranes with a pore size close to 30 kDa are obtained by controlling the membrane manufacturing variables.

García-Ivars et al. (2015) developed several investigations where PES membranes with a molecular cut-off size between 25 and 30 kDa were made [26]. In other studies, the membranes were manufactured with high-impact polystyrene (virgin and recycled), yielding similar conclusions: the membranes have a molecular cut-off size around 40 kDa [27].

As a result of the above studies, the authors have decided to use a PEG of molecular weight 35 kDa as feed for the pilot plant characterisation tests of the manufactured membranes. To the best of our knowledge, this is the first time that hybrid PES/AC membranes were synthesised and characterised using the process conditions, the materials, and the techniques employed in this study.

2. Materials and Methods

2.1. Chemicals and Materials

Polyethersulfone (PES) Ultrason® E 2010 (BASF, Ludwigshafen, Germany) was employed as a base polymer and N,N′-dimethylacetanamide (DMA) was used as a solvent. The non-woven commercial support utilised was Viledon FO-2402 (Freudenberg, Germany). PEG solutions were made by employed 35 kDa particles. These solutions had a concentration of $20 \text{ g} \cdot \text{L}^{-1}$ to study the flux and membrane recovery after fouling. DMA and PEG were acquired from Sigma Aldrich (Darmstadt, Germany). Osmotized water was employed in this study, and a 0.1 M solution of NaOH with a pH of 12 (purchased from Panreac, Vallès, Spain) was used for membrane cleaning.

Three commercial activated carbons were used for this investigation. Firstly, Norit R2030CO2, referred to as Norit R, is a peat-based activated carbon supplied by Cabot (Cabot Corporation, Rotterdam, The Netherlands). Norit PK is an activated carbon supplied by Merck (formerly Sigma Aldrich, Gillingham, UK), and, lastly, powder-activated charcoal

was supplied by PanReac AppliChem (Barcelona, Spain), referred to as PANREAC. Norit R and Norit PK, provided in granular form, were ground to powder form using a mortar and pestle, and then sieved to obtain particles smaller than 1 mm diameter.

2.2. Synthesis of Membranes

Ten activated carbon membranes (M0–M9) were prepared using the NIPS method as shown in Table 1. Different concentrations of AC were dispersed in DMA. The composition of all PES-AC/DMA solutions was 20/80 wt. (%). In order to prevent agglomeration, these solutions were prepared under mechanical stirring at 20 °C for at least 24 h until a homogenous solution was obtained. Afterward, the solutions were uniformly poured over the non-woven support by employing a film applicator with a 200 μm casting knife and immersed in a coagulation bath (non-solvent: osmotized water at 15 °C). The formed membranes were kept in the bath for at least 10 min to guarantee precipitation. Subsequently, they were washed to remove residual DMA and maintained in osmotized water for additional analysis.

Table 1. Membrane preparation characteristics.

Membrane	AC, wt. (%)		PES, wt. (%)	DMA, wt. (%)
M0	-	-	20.00	
M1	PANREAC	0.10	19.90	
M2	PANREAC	0.50	19.50	
M3	Norit R	0.10	19.90	
M4	Norit R	0.50	19.50	80.00
M5	Norit R	1.00	19.00	
M6	Norit R	1.50	18.50	
M7	Norit R	2.00	18.00	
M8	Norit PK	0.10	19.90	
M9	Norit PK	0.50	19.50	

2.3. Activated Carbon Characterisation

N_2 isotherms at -196 °C and CO_2 isotherms at 0 °C were measured for the activated carbons using a Micrometrics ASAP 2020 analyser. From the isotherm experiments, key textural properties were calculated. In terms of N_2 isotherms, Pore Size Distribution (PSD) data were obtained using Density Functional Theory (DFT) assuming a split pore geometry. Specific surface area was calculated using the Brunauer–Emmet–Teller (BET) equation, total pore volume was calculated using Gurvich's Law, and micropore volume was calculated using the Dubinin–Radushkevich (DR) equation [28]. The mesopore volume was calculated as the difference between the micropore volume and the cumulative pore volume at a pore size of 50 nm. CO_2 isotherms at 0 °C were used to determine the presence of ultramicropores (<0.7 nm), with the DR equation again used for calculating ultramicropore volume [29].

The thermal stability of the activated carbons was measured using a Mettler Toledo 3+ Thermogravimetric Analyser (TGA). Approximately 20 mg of the sample was placed in an aluminium oxide crucible before insertion into the TGA furnace. Samples were subjected to a heating ramp (10 °C min^{-1}) under inert conditions provided by feeding N_2 (50 NmL·min $^{-1}$)). The heating ramp was conducted from 25 to 1000 °C and the mass loss (%) was recorded with increasing temperature [30]. Also obtained from these data was the derivative thermogravimetric curve (DTG), a curve that shows the rate of mass loss with respect to time (% s $^{-1}$) against temperature (25–1000 °C).

2.4. Filtration Experiments

Membrane permeability was characterised based on osmotized water flux, where flat-sheet membranes were preserved in deionised water and placed in the dead-end XFUF 076 01 stirred cell (Merck Millipore, Burlington, MA, USA). The membranes with an effective

area of 27.3 cm^2 were used to measure the water flux under different transmembrane pressures (TMPs), increasing from 0.5 to 2.0 bar at a constant flow rate of 250 L·h^{-1} and 20 °C. The weight of the permeate water was measured by balance every 30 s and deionised water flux was calculated using Equation (1) [31,32] below:

$$J_w = \frac{V}{A_m \cdot \Delta t} \tag{1}$$

where J_w is the deionised water flux (L·m^{-2}·h^{-1}), V represents the permeate volume (L), A_m is the effective area of the membrane (m^2), and Δt is the test time (h).

The intrinsic membrane resistance (R_m) was obtained by isolating this term in Darcy's law using Equation (2) [31,32]:

$$R_m = \frac{TMP}{\mu \cdot J_w} \tag{2}$$

where μ is the dynamic water viscosity (Pa·s) at the operation temperature.

Alternatively, Equation (2) can be expressed as follows:

$$J_w = K \cdot TMP \tag{3}$$

where K is permeability (L·m^{-2}·h^{-1}·bar^{-1}) and combines both viscosity and membrane resistance terms.

The same filtration setup was employed for PEG permeation essays to test the membrane removal performance. Permeate flux (J_{PEG}, L·m^{-2}·h^{-1}) and rejection index were measured using 20 g·L^{-1} of PEG solution. The filtration tests were performed at 20 °C and 1 bar. The rejection index of the PEG original solution and the permeate concentrations were measured using a refractometer (ATAGO, RX-5000). The rejection index was calculated using Equation (4) below [31]:

$$R = \left(1 - \frac{C_p}{C_f}\right) \cdot 100 \tag{4}$$

where R is the rejection index (%), C_p is permeate concentration (g·L^{-1}), and C_f represents the feed concentration (g·L^{-1}).

After PEG solutions were tested in the different membranes, they were immersed in deionised water for at least 24 h to remove superficial fouling from the membranes and tested again with osmotized water. Water flux was then compared by employing the flux recovery ratio (FRR) as follows:

$$FRR \ (\%) = \frac{J_r}{J_w} \cdot 100 \tag{5}$$

where J_r (L·m^{-2}·h^{-1}) is the osmotized water flux after rinsing and J_w (L·m^{-2}·h^{-1}) is the original osmotized water flux.

An additional cleaning of the membranes was applied using a basic solution (NaOH, pH = 12) to remove the non-superficial PEG deposition. To analyse the fouling phenomenon, different membrane resistances were defined using Equations (6)–(9) [27]:

$$R_T = R_m + R_{rev} + R_{irr_{chem}} + R_{irr_{non\ recoverable}} \tag{6}$$

$$R_{rev} = \frac{\Delta P}{\mu \cdot J_{PEG}} - R_m - R_{irr_{chem}} - R_{irr_{non\ recoverable}} \tag{7}$$

$$R_{irr_{chem}} = \frac{\Delta P}{\mu \cdot J_r} - R_m - R_{irr_{non\ recoverable}} \tag{8}$$

$$R_{irr_{non\ recovered}} = \frac{\Delta P}{\mu \cdot J_c} - R_m \tag{9}$$

where R_T (m^{-1}) refers to the total filtration resistance, R_{rev} (m^{-1}) is the reversible fouling that could be reduced by physical cleaning, J_{PEG} (L·m^{-2}·h^{-1}) is the permeate flux of the filtrations of PEG solutions at steady state, $R_{irr_{chem}}$ (m^{-1}) is the irreversible fouling which determines the flux loss in the permeate stream that would be recovered by chemical cleaning, $R_{irr_{nonrecoverable}}$ (m^{-1}) includes the irreversible fouling that could not be recovered, and J_c (L·m^{-2}·h^{-1}) is the osmotized water flux after applying the chemical cleaning.

2.5. Membrane Characterisation

Field emission scanning electron microscopy (FESEM) was carried out to analyse cross-sectional morphology of the membrane, as well as the activated carbon structures themselves.

Activated carbon polysulfone membranes were fractured in liquid nitrogen. All the samples were sprayed with a conductive carbon layer before FESEM assays. Morphological examinations were obtained by using a ZEISS Ultra-55 (Jena, Germany) Scanning Electron Microscope. The analytical conditions were as follows: 2 kV accelerating voltage; 5.3 mm working distance.

Additionally, surface hydrophilicity of the membranes was characterised in terms of porosity and equilibrium water content (EWC). Average porosity (ε) was defined by the wet–dry weighting method. Initial wet weight (W_W) was obtained after 15 min submersion in osmotized water and by removing the leftover water on the membrane surface, whereas the dry weight (W_D) was acquired after drying the samples for 6 h at 50 °C. These parameters were calculated as shown in the following equations (Equations (10) and (11) [27]):

$$EWC\ (\%) = \frac{W_W - W_D}{W_W} \cdot 100 \tag{10}$$

$$\varepsilon\ (\%) = \frac{W_W - W_D}{S_m \cdot \rho_W \cdot \delta} \cdot 100 \tag{11}$$

where W_W and W_D are the wet and dry weight of the samples (kg), respectively; ρ_W is the water density at operating conditions (kg·m^3); S_m is the membrane surface analysed (m^2); and δ is the membrane thickness (m).

Lastly, pore size of the activated carbon polysulfone membranes was obtained by employing the Guerout–Elford–Ferry equation [27,33] in order to estimate the true pore size. It is shown in Equation (12) using the water-filtration velocity method.

$$r_m = \sqrt{\frac{(2.9 - 1.75 \cdot \varepsilon) \cdot 8 \cdot \mu \cdot \delta \cdot Q_w}{\varepsilon \cdot A_m \cdot \Delta P}} \tag{12}$$

where Q_w is the water flow (m^3·s^{-1}) and ε is the porosity calculated as shown in Equation (11).

2.6. Statistical Analysis

To analyse the effect of AC on membrane properties, a one-way ANOVA (Statgraphics Centurion XVIII) statistical analysis of measured permeabilities was conducted. The 95% confidence level was fixed to obtain the F-ratio and *p*-value.

3. Results and Discussion

3.1. Filtration Experiments and Membrane Characterisation

Permeation flux (J) is one of the principal parameters to define the amount of fluid crossing the synthesised membranes as a function of the pressure applied. Accordingly, the membrane's water permeability was characterised. As filtration experiments were carried out, permeation flux was determined at the initial conditions (immediately after manufacturing the membranes), after rinsing, and finally after chemical cleaning, as shown in Table 2.

Table 2. Water permeability (K) and PEG rejection index (R) of the membranes prepared with different activated carbon loadings (wt. (%)).

Membrane	K (L·m^{-2}·h^{-1}·bar^{-1})			R (%)
	Initial Conditions	After Rinsing	After Chemical Cleaning	
M0	280.35	189.14	270.70	62.92
M1	159.50	103.58	145.09	78.28
M2	187.95	128.31	154.21	62.50
M3	234.10	176.53	255.61	62.14
M4	219.29	117.28	160.97	80.34
M5	156.26	205.65	215.71	50.82
M6	256.86	273.67	256.43	49.59
M7	294.99	205.60	249.57	55.66
M8	329.24	261.40	278.93	48.56
M9	312.63	273.30	289.22	46.61

It is observed that Norit R-doped membranes (M3 to M7) show intermediate permeability values. In these membranes, uniform AC/PES polymer blends are observed, even when the activated carbon loading is higher (from 0.1 to 2.0 wt. (%) activated carbon added). On the contrary, PANREAC and Norit PK membranes do not coexist homogenously for activated carbon loadings over 0.5 wt. (%). The permeability values obtained after rinsing show a slight decrease compared to the initial conditions. The previously described chemical cleaning allows for a greater permeability recovery so that it approaches as close to the initial permeability as possible. This theoretical situation is obtained for the reference membrane (M0) and for all membranes manufactured with AC PANREAC (M1 and M2), and for those manufactured with AC Norit PK (M8 and M9). The situation is not analogous for all membranes manufactured with AC Norit R. For M3, a permeability value greater than the initial one is reported after chemical cleaning. This peculiarity may be because the basic solution has been able to remove some fewer stable fractions from the membrane's internal structure. M5, in addition, has a very peculiar behaviour; as cleaning is applied, a progressively superior permeability is found, in all cases being larger than the initial one.

The rejection indexes (%) shown in Table 2 are also displayed in Figure 1, which shows both the rejection of the PEG solutions and the obtained flux for each membrane tested. It can be observed that PEG fluxes are smaller than those obtained when osmotized water is employed, which is typical. In general terms, solution permeation flux does not present significant variations.

This combined graphic denotes several conclusions. Firstly, Norit PK membranes could not reach 50%, showing the lowest PEG rejection rates (46.61 to 48.56), suggesting that Norit PK might not be the most effective AC for solute rejection. PANREAC membranes showed a moderate to high rejection. An increase in wt.% from 0.10 (M1) to 0.50 (M2) resulted in a decrease in the rejection rate from 78.28 to 62.50. This indicates that a lower wt.% might be more effective with PANREAC membranes. The opposite situation took place with Norit R membranes presenting the highest rejection for 0.5 wt. (%) and consecutively a notorious reduction for higher concentrations (from wt.% = 1.00 to wt.% = 2.00). Therefore, the performance of these membranes might be highly dependent on other factors such as wt.%. M4, which incorporates Norit R at a concentration of 0.5 wt.%, exhibits a peak rejection rate for the compound under investigation. This optimal point is achieved, leading to a minimisation of membrane fouling and consequently enhancing its rejection capability. Specifically, the reduction in the accumulated cake layer on the membrane surface contributes to this improved performance. This observation emphasises the importance of carefully controlling the activated carbon concentration in the membrane formulation to achieve superior rejection rates.
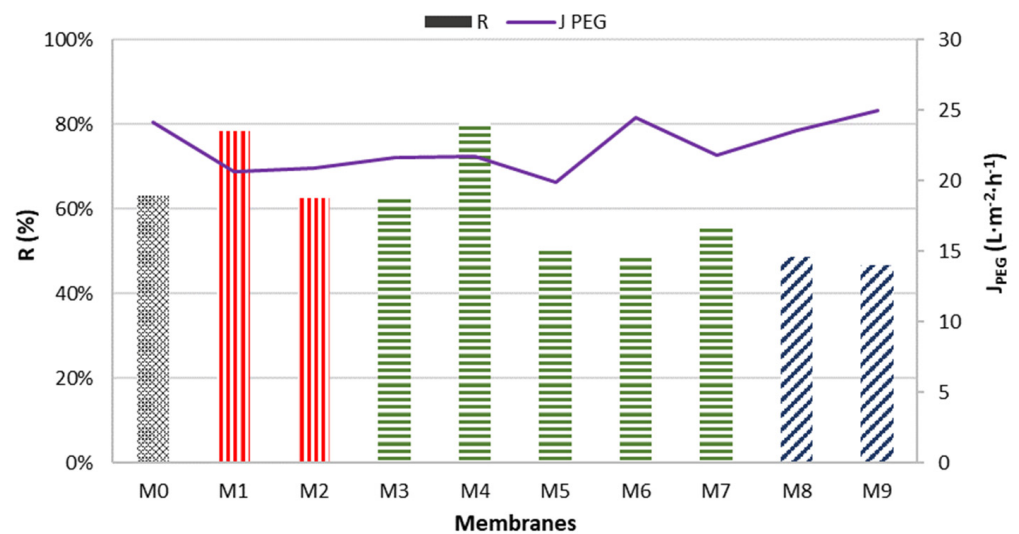
Figure 1. Rejection index, R (%) (above in vertical bars), and PEG flux, J_{PEG} (L·m^{-1}·h^{-1}) (line), for each membrane. Grey bar: membrane without AC; Red bar: PANREAC AC membrane; Green bar: Norit R AC membrane; Blue bar: Norit PK membrane.

In conclusion, both the type of AC and the wt.% appear to influence the rejection rates of the membranes significantly. Nevertheless, the relationship between these factors and the membrane performance is complex and is not linear. Further studies could help elucidate these relationships and optimise the membrane manufacturing process.

3.2. Statistical Analysis

To analyse the results obtained in the physical characterisation of the membranes tested, one-way ANOVA analysis for the values measured was employed, using the different activated carbons added and their quantities (from 0 to 0.5 wt. (%)) as factors. The activated carbon was found to be statistically significant (F = 36.00; *p*-value = 0.0024), while the weight percentage added to the solution was not statistically significant.

The initial permeability of the membranes tested is shown in the Tukey's diagram displayed in Figure 2. The plain membrane (M0, no AC) was used as a reference sample, and membranes with ACs added at different wt. (%) were referenced according to the type of activated carbon. Membranes synthesised with PANREAC activated carbon presented the lowest permeability of the membranes tested.
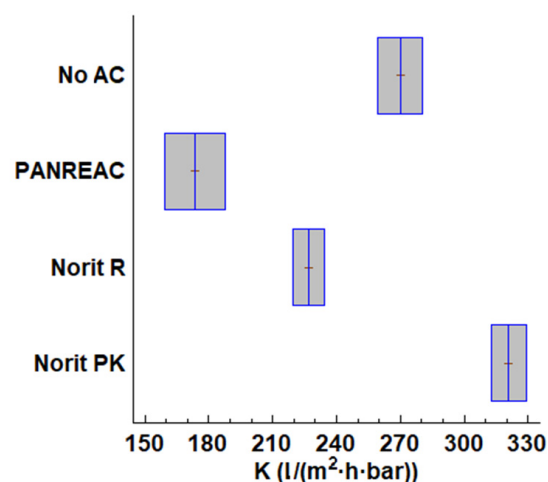

Figure 2. Tukey's diagram for initial membrane permeability for each type of activated carbon added.

Similarly, Norit R-activated carbon membranes exhibited permeability value ranges smaller than that of the control membrane. This may be due to the formation of closer pores within PANREAC and Norit R membranes. On the contrary, Norit PK membranes showed greater permeability values than that of the control membrane, indicating that the pores created were more open in this case.

3.3. Activated Carbon Characterisation

The textural properties of the ACs employed in the synthesis of the hybrid PES/AC membranes were obtained from the N_2 and CO_2 adsorption isotherms, measured at -196 and $0\,^\circ C$, respectively. Figure 3 displays the N_2 isotherms. The shape of the PANREAC and Norit PK isotherms describes Type I IUPAC behaviour, thus indicating that they are mainly microporous carbons. In the case of Norit R, the isotherm shape and hysteresis loop formed at relative pressures above 0.4 indicate the Type IV isotherm in the IUPAC classification. This is associated with the presence of larger pores (mesopores: 2 nm < diameter < 50 nm) within the activated carbon.
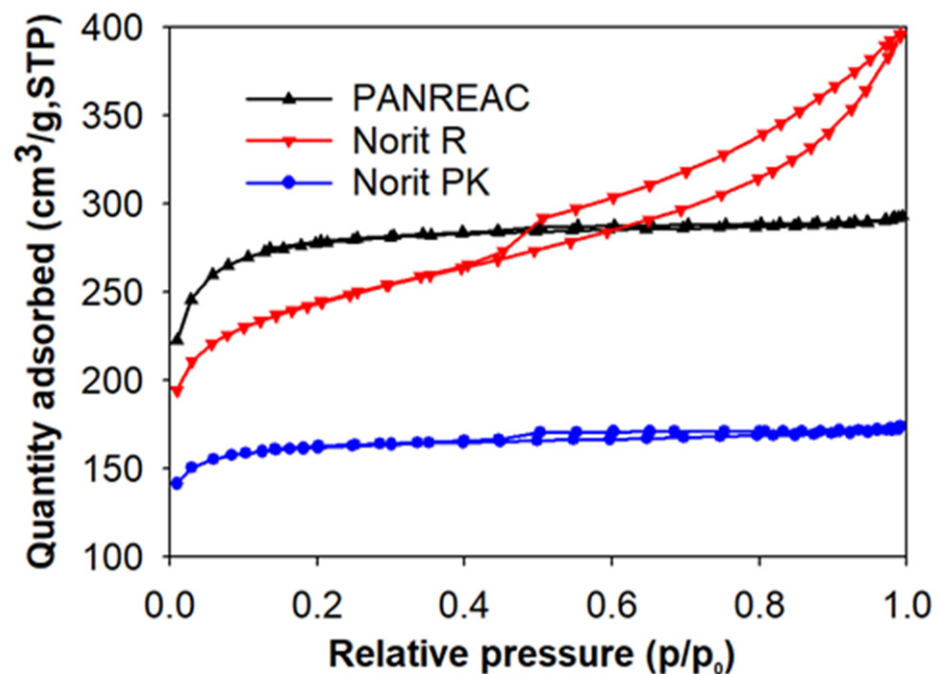
Figure 3. N_2 adsorption–desorption isotherms of the activated carbons measured at $-196\,^\circ C$.

The behaviour identified in the isotherms is reflected in textural property calculations recorded in Table 3. These results show that PANREAC and Norit R possess substantial specific surface areas (990 and 870 m^2/g, respectively), while Norit PK possesses a more moderate specific surface area (578 m^2/g). In terms of pore structure, Norit PK and PANREAC are more similar, possessing a high microporosity presence (>90%) with respect to pore volume. Norit R, as suggested from N_2 adsorption data where it adsorbed the most N_2 at $-196\,^\circ C$, possesses the largest total pore volume (0.62 cm^3/g) but shows a lower micropore volume. Pore size dimensions vary amongst the sorbents. PANREAC has a similar average pore width to Norit PK (1.83 and 1.86 nm) but shows wider micropores based on the calculated average micropore width (1.76 against 0.98 nm). Norit R does possess an intermediate average micropore width (1.41 nm); however, its substantially larger average pore width (2.84 nm) is indicative of its greater mesopore presence compared to the other activated carbons.

Table 3. Textural properties of the activated carbons calculated from the N_2 and CO_2 adsorption isotherms measured at $-196\ ^\circ C$ (a–f) and CO_2 at $0\ ^\circ C$ (g–h), respectively.

Sample	S_{BET} [a] (m^2/g)	W_T [b] (cm^3/g)	W_0 [c] (cm^3/g)	W_{meso} [d] (cm^3/g)	D [e] (nm)	L_0 [f] (nm)	$W_{0,\ ultra}$ [g] (cm^3/g)	$L_{0,ultra}$ [h] (nm)
PANREAC	990	0.45	0.44	0.07	1.83	1.76	0.23	0.61
Norit R	870	0.62	0.37	0.10	2.84	1.41	0.26	0.64
Norit PK	578	0.27	0.25	0.05	1.86	0.98	0.26	0.63

[a] Specific surface area; [b] total pore volume; [c] total micropore volume; [d] total mesopore volume; [e] average pore diameter; [f] average micropore width; [g] ultramicropore volume; [h] average ultramicropore width.

Pore Size Distribution is shown in Figure 4, presenting an augmentation on the left for the range of 1–10 nm that allows microporosity identification. The results confirm the notable mesopore presence in Norit R, while PANREAC and Norit PK possess a predominantly microporous distribution of pore sizes. The PSD data show a slight presence of macropores (pore diameter > 50 nm) in the size range of 100–140 nm for Norit PK and 115–140 nm for Norit R, whereas a slight macropore presence is detected for PANREAC in the size range of 50–220 nm. Given its substantial mesoporosity, Norit R may be particularly well suited for applications requiring the rapid transport of larger molecules. On the other hand, PANREAC and Norit PK, characterised by their pronounced microporosity, may be more apt for applications that demand high adsorption capacity. The existence of macropores in all these activated carbons could potentially enhance their overall performance by enabling the migration of molecules to the smaller pores. In general, an optimally developed pore structure with a balanced distribution of micro- and mesopores is advantageous for most applications, as it guarantees a high surface area for adsorption and good transport properties [34].
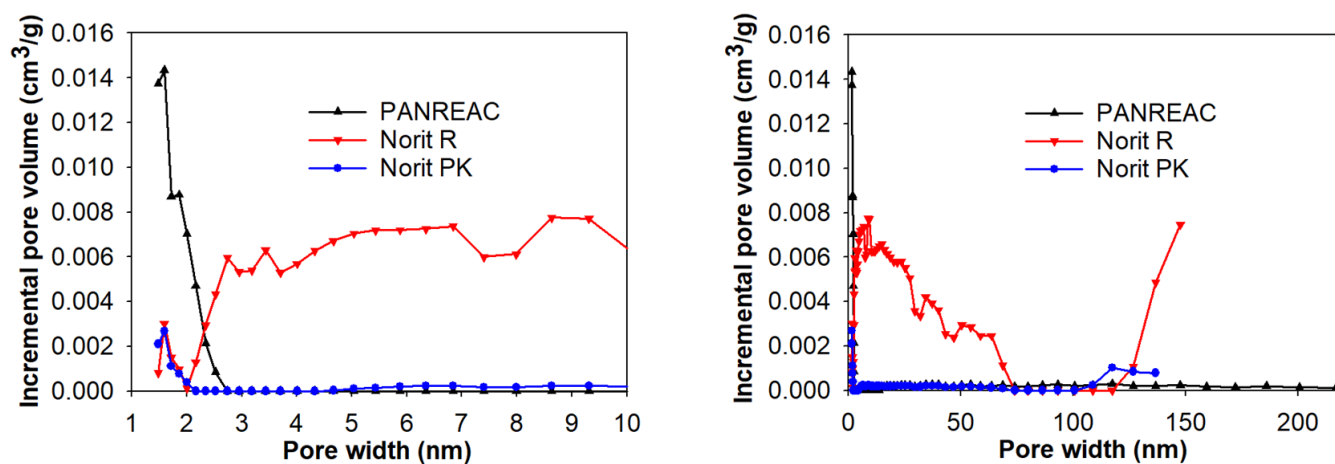
Figure 4. Pore Size Distribution (PSD) of the activated carbons calculated from the N_2 adsorption–desorption isotherms. Augmentation scale ranges from 1 to 10 nm on the (**left**) and the full scale ranges from 0 to 200 nm on the (**right**).

Figure 5 depicts the CO_2 adsorption isotherms of all three activated carbons. They all show similar CO_2 adsorption capacities. Calculations in Table 3 show the activated carbons possessing similar ultramicropore (diameter < 1 nm) characteristics. Thus, it confirms that narrow-pore characteristics show minimal variations. Both micropores and mesopores are considered suitable pore sizes in AC for adsorption and filtration applications [13], which these activated carbons possess predominantly. Overall, the three ACs, despite being different, exhibit similar CO_2 adsorption capacities and ultramicropore characteristics,

with PANREAC being the one which shows a slightly wider micropore size distribution, reflected in its largest average micropore width (L_0).
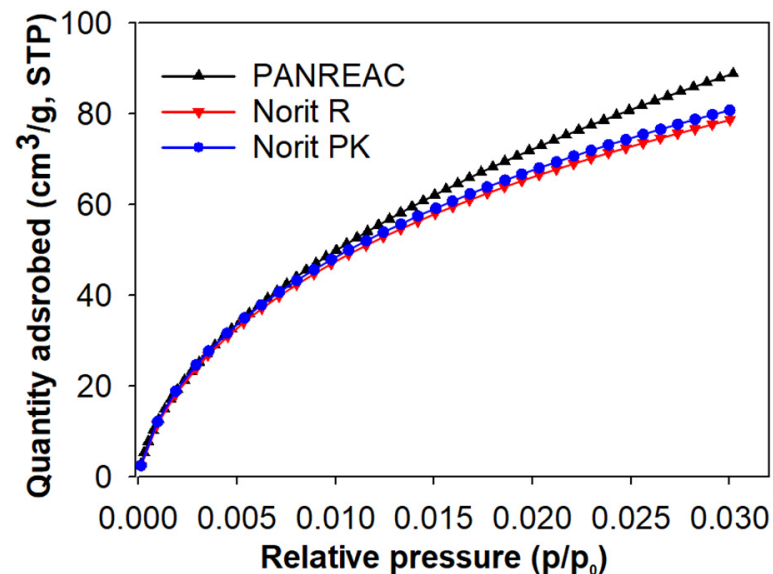

Figure 5. CO_2 adsorption isotherms of the activated carbons measured at 0 °C.

Figures 6 and 7 show the thermal stability profiles and the corresponding DTG curves of the activated carbons, respectively. Mass changes in the temperature range of 30–140 °C are associated with moisture loss [35]. These represent the largest mass losses experienced for all three activated carbons, which are accentuated by the largest peaks in the DTG curves obtained for each activated carbon as shown in Figure 7. This equates to mass losses of 6% for PANREAC and 3% for Norit PK and Norit R, respectively (Figure 6). Mass losses remain slight up to the maximum temperature of 1000 °C. Overall, both Norit R and Norit PK experienced mass losses of 8 wt. (%), while PANREAC showed a total of 12 wt. (%) in mass losses. These mass losses in the higher temperature range have once been associated with the removal of functional groups such as carboxylic acids, phenols, carbonyl groups, quinones, and pyrones [35]. These relatively slight mass losses due to thermal degradation thus show that all the activated carbons possess great thermal stability.
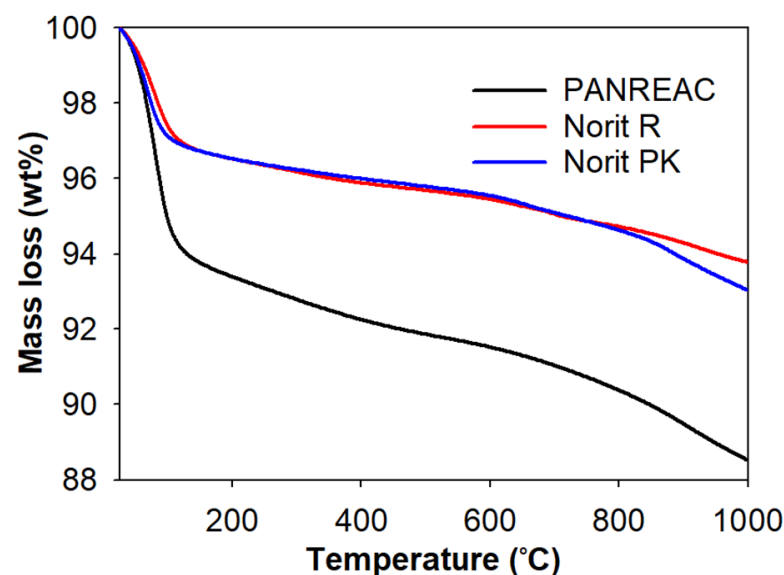

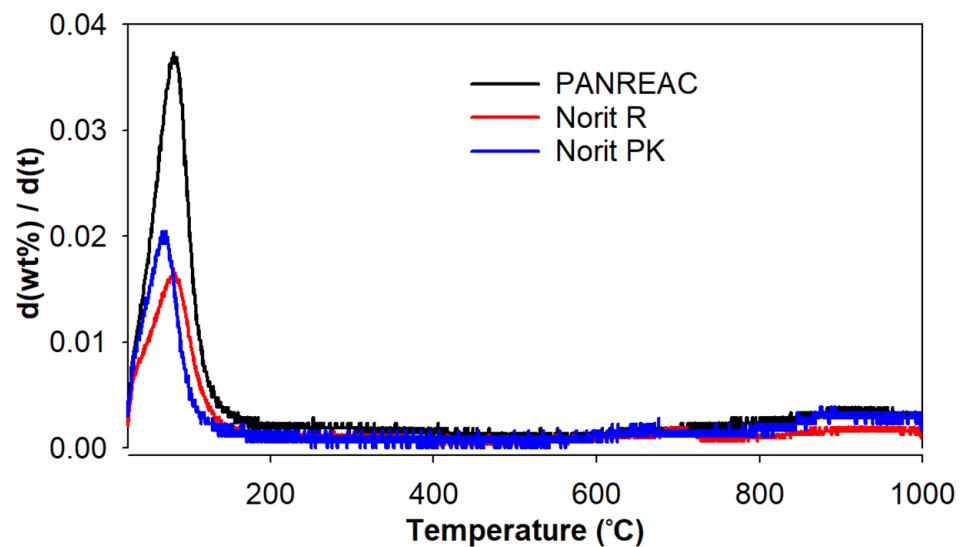**Figure 6.** Activated carbon TGA thermal stability curve.

Figure 7. Activated carbon DTG curve.

3.4. Activated Carbon Influence on Membrane Behaviour

Correlations between both AC characterisation and membranes performance were analysed. For that, all key textural properties presented in Table 3 were plotted against the rejection index (R,%). However, just S_{BET}, W_0, and L_0 reported accurate relations (see Figure 8).
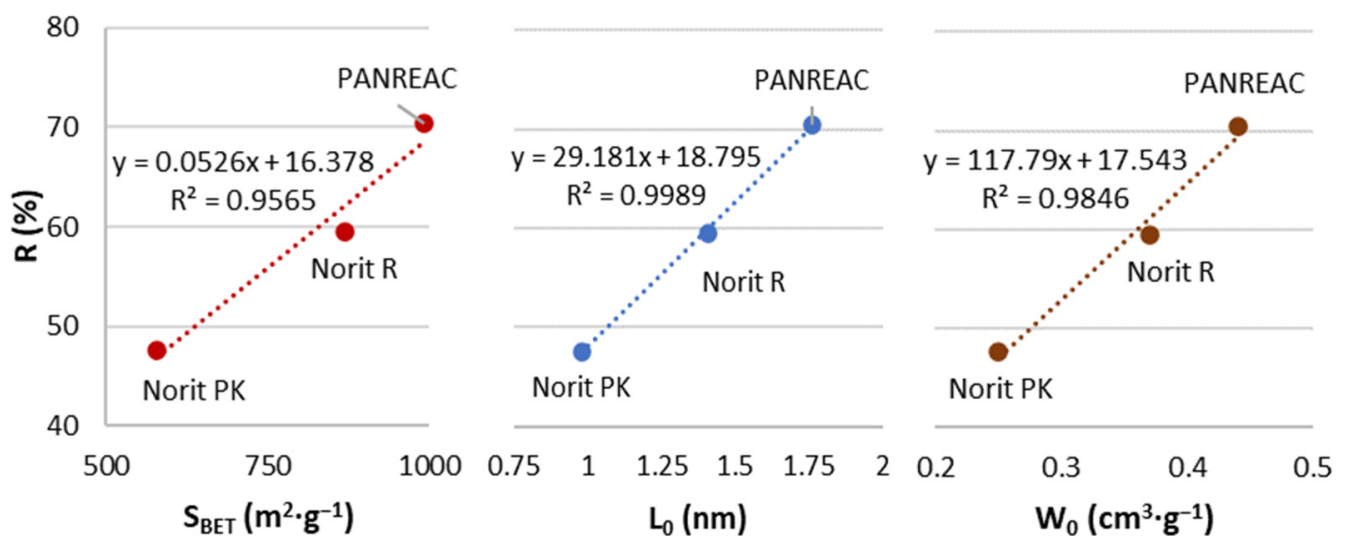

Figure 8. Correlations between specific surface area (S_{BET}), total micropore volume (W_0), and average micropore width (L_0) with rejection index (R).

The authors kept in mind the incorporation of AC in the membrane structure. Therefore, two phenomena could be involved: on the one hand, the adsorption process that occurs in this compound; on the other hand, an additional effect was observed—the pore former in the membrane structure. In this way, a relationship between the AC characteristic pore (micropore–mesopore) and the resulting porous structure of the membrane was obtained.

The trends observed indicate that when the values of S_{BET}, L_0, and W_0 increase, so does the rejection index. As a result, the membrane system rejects better the pollutant. Wider micropores, as well as higher micropore volumes, lead to larger PEG sorption capacities, as well as to larger membrane separation capacities. Moreover, this increase in rejection

index is also observed for those ACs that have higher specific surface areas (S_{BET}). For instance, PANREAC AC membranes showed the highest rejection rate mean values due to their highest S_{BET} (990 m^2/g). The larger specific surface in the AC is related to a more extensive area within the material, so physical and chemical processes such as sorption can take place. The opposite situation is observed with Norit PK membranes due to the smaller S_{BET} (578 m^2/g) exhibited by this AC, which appears to lead to rejection index values below 50%. Overall, it can be concluded that rejections are probably the result of the combined effects of the AC characteristics, the wt. (%) of AC added to the membrane, and the way they interact and spread within the membrane. What is certainly apparent from the positive trends observed in Figure 8 is the great impact that the AC textural properties have on the rejection index values.

Additionally, when adding ACs into a membrane, one important performance parameter that should not become compromised is consistency. In PANREAC and Norit PK membranes, the shown trend is a reduction in R (%) when increasing the wt. (%) of AC, which agrees with the behaviour reported by Liu et al. (2020), where the maximum rejection appeared at the minimum additive composition, and it decreased gradually [36]. However, Norit R membranes presented the opposite performance, and they reached an unexpected optimum R value at 0.5 wt. (%), which then decreased with greater AC additions. These opposite performances observed with Norit R membranes are likely correlated to the ability of Norit R to form a homogenous coexistence with higher AC loadings, different from the other analysed cases.

3.5. Fouling Assays

To further interpret the results obtained, membrane resistances have been plotted in Figure 9 in relation to the total resistance of the membrane (R_T). Intrinsic membrane resistance (R_m), reversible resistance (R_{rev}), chemical irreversible resistance ($R_{irrev\ chem}$), and irreversible non-recoverable resistance ($R_{irrev\ non\ rec}$) were calculated as explained in Section 2.4, presented as a ratio of the total resistance. This way, a quantitative evaluation can be performed for every contribution. The first aspect to emphasise is the remarkable influence of PEG. In the present study, at least 80% of the total resistances refer to reversible fouling in all cases. No recoverable resistances are minimum, and intrinsic resistances are higher than those associated with chemical recovery. Independently of membranes, these results suggest that the low contribution of irreversible resistances is due to PEG temporary fouling.
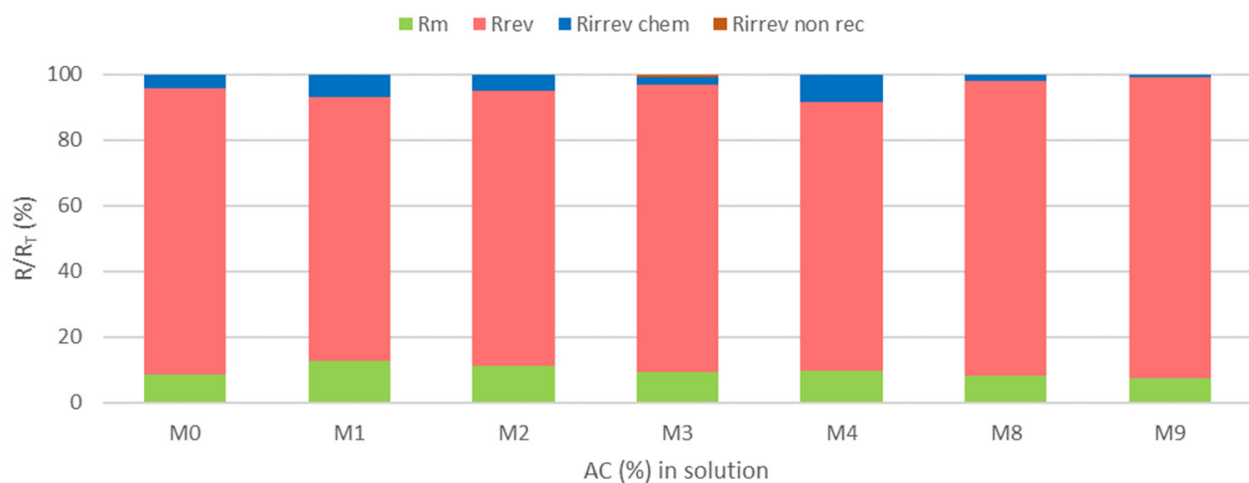
Figure 9. Analysis resistance contribution to the total. R_T, total resistance; R_m, intrinsic membrane resistance; R_{rev}, reversible resistance; $R_{irrev\ chem}$, chemical irreversible resistance; and $R_{irrev\ non\ rec}$, irreversible non-recoverable resistance. Note: M0 (no AC); M1 (PANREAC, 0.10%); M2 (PANREAC, 0.50%); M3 (Norit R, 0.10%); M4 (Norit R, 0.50%); M8 (Norit PK, 0.10%); M9 (Norit PK, 0.50%).

The membrane fluxes from the fouling experiments measured at 1 bar of TMP are presented in Figure 10, reinforcing the results discussed and conclusions made previously. The rinsing and chemical cleaning denote partial or total recovery of the original fluxes.
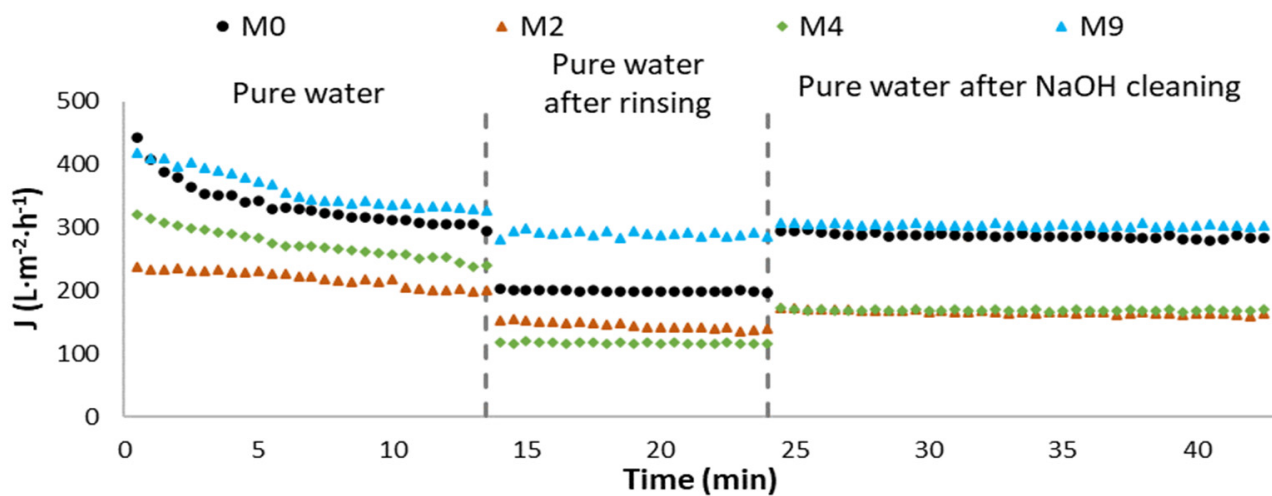
Figure 10. Time-dependent flux (J) until stabilisation of the AC/PES membrane. Initial filtration is presented, and then the same filtrations are exposed after rinsing and after basic cleaning. Applied pressure: 1 bar. Rinsing performed after 20 g·l^{-1} PEG solution filtrations were completed. Note: M0 (no AC); M2 (PANREAC, 0.50%); M4 (Norit R, 0.50%); M9 (Norit PK, 0.50%).

Fouling experiments with PEG 35 kDa were conducted to evaluate the rejection during filtration time. As tests were performed with a 35 kDa particle, the flux rapidly declined due to the fast accumulation of these particles on the surface and inside the membrane pores. After this adaptation, a steady state was reached, and stable values were obtained.

These results are justified as a function of the pore size of the membrane. If the pore is small, the particles enter inside the finger of the structure, causing sticky fouling and pore blockage, whereas if the pore is large, as in the case of activated carbon Norit PK, a superficial fouling appears, forming a pseudo-membrane layer, and the fouling is removed more easily, having a greater recovery of the permeate flow [37].

With all the results discussed above and considering that there is no correlation found between the total micropore volume and the membrane permeability, it can be assumed that the AC textural parameter that influences the membrane permeability the most is the micropore size (average micropore diameter).

We can conclude that the characteristics of the added ACs lead to a modification in the membrane's macroscopic performance, such as permeability or R index, as seen in Table 2.

*3.6. Equilibrium Water Content, Porosity, and Pore Size*

Results of equilibrium water content (EWC) were obtained for the synthesised membranes as shown in Table 4.

Table 4. Equilibrium water content (EWC) obtained for each membrane. Note: M0 (no AC); M1 (PANREAC, 0.10%); M2 (PANREAC, 0.50%); M3 (Norit R, 0.10%); M4 (Norit R, 0.50%); M5 (Norit R, 1.00%); M6 (Norit R, 1.50%); M7 (Norit R, 2.00%); M8 (Norit PK, 0.10%); M9 (Norit PK, 0.50%).

	M0	M1	M2	M3	M4	M5	M6	M7	M8	M9
EWC (%)	38.53 ± 1.73	31.42 ± 0.70	34.93 ± 5.16	37.12 ± 1.96	35.93 ± 2.97	36.98 ± 5.52	37.87 ± 1.25	41.08 ± 1.89	37.19 ± 0.09	45.85 ± 4.07

The anticipated performances of the membranes suggested that the addition of compounds to the polymeric solution would result in higher porosities and water content in

the membranes [27], as can be seen in Figure 11. Looking at the data, we see that the EWC values range from 31.42% to 45.85%. The membrane M9, with an EWC of 45.85%, shows the highest water content among all the membranes. This membrane (0.50% wt. Norit PK) could make the enhancement in water absorption possible, leading to a higher EWC, meaning more absorption sites for water. However, it is important to note that several factors can influence EWC, including the membrane's intrinsic properties. Therefore, while the type and amount of AC are significant, they are part of a complex interplay of factors determining the EWC. The increment in the EWC parameter resulted in a more hydrophilic surface. This similar tendency has been previously reported with progressive additive incorporation, as shown in the table above [38]. EWC and porosity for Norit PK membranes were largest among all the produced membranes, as expected from Table 2—results where permeabilities were noticeably higher. In the opposite situation, PANREAC membranes prevent water from entering within its structure. EWC values are lower for 0.1 wt. (%) AC membranes than for the reference one (M0), and this value increases as the AC mass increases. The exception appears within M4 (Norit R—0.5%) and its minor EWC value in comparison to other Norit R membranes. Therefore, the relation between this parameter and the rejection index explained in Section 3.1 should be highlighted. Nevertheless, regarding ε values, no relevant differences can be linked to AC wt. (%).
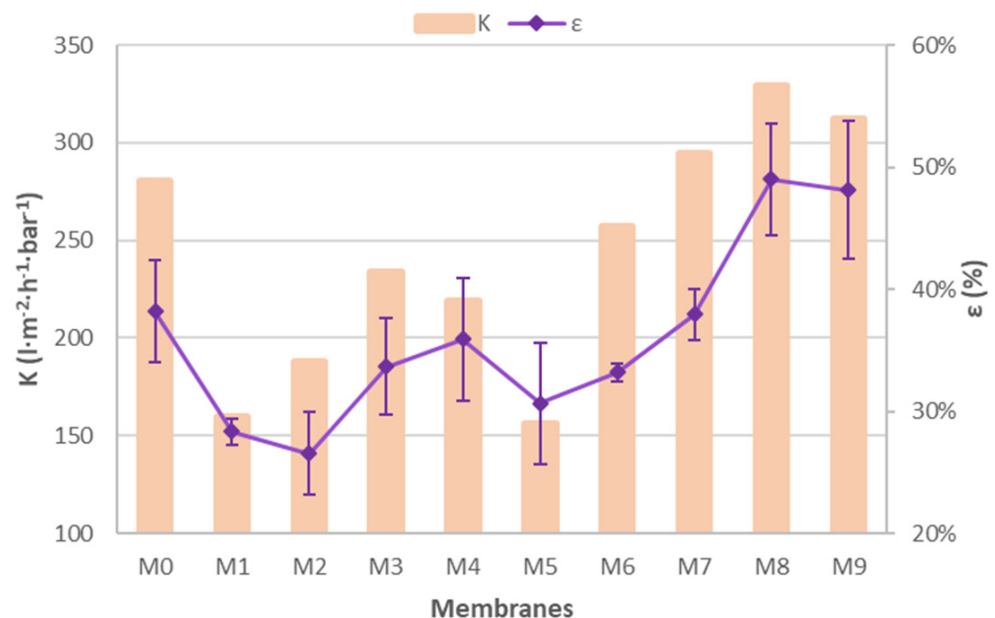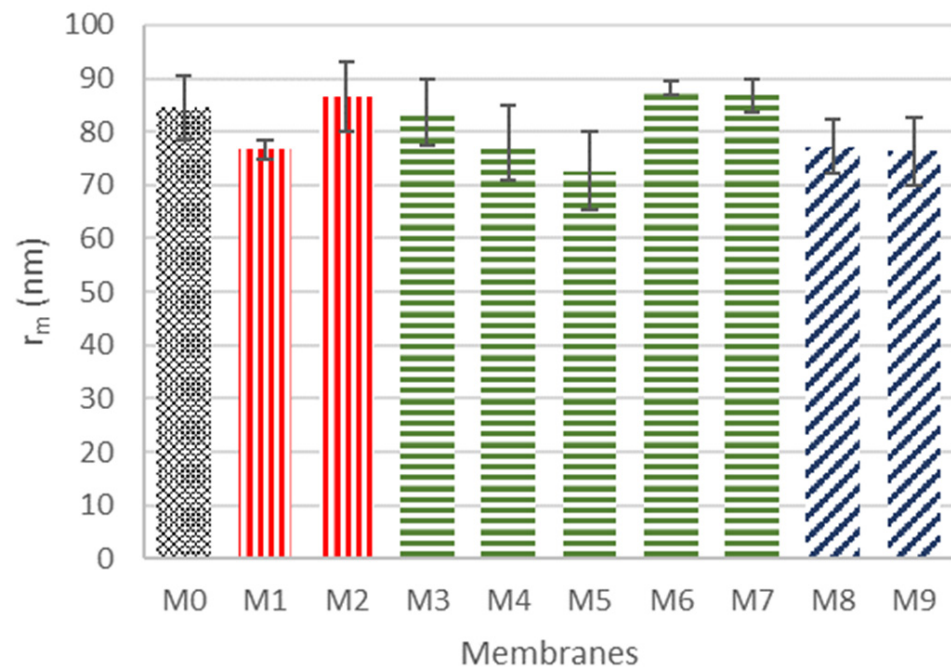

Figure 11. Porosity (ε) of each membrane compared to its permeability (K). Note: M0 (no AC); M1 (PANREAC, 0.10%); M2 (PANREAC, 0.50%); M3 (Norit R, 0.10%); M4 (Norit R, 0.50%); M5 (Norit R, 1.00%); M6 (Norit R, 1.50%); M7 (Norit R, 2.00%); M8 (Norit PK, 0.10%); M9 (Norit PK, 0.50%).

Figure 12 shows the average pore size for each membrane. Note that the different shapes and colours in the figure are used to distinguish the AC type added to the membranes. Similar average pore size values are obtained for all the synthesised membranes, and no correlation is observed with AC type or the wt. (%) of AC added. The membrane pore sizes obtained are strictly related to permeabilities of the membranes, while no significant variations in pore sizes are linked to their rejection capacity.

Nevertheless, different authors reported significantly lower pore sizes than those obtained in this work. Wang et al. (2019) described values between 15 and 30 nm using 15–20 wt. (%) of PES or polysulfone (PSF) [39]. Also, Wu et al. (2008) studied phase-inversion membranes by adding nanotubes of TiO_2 to polyvinylidene fluoride (PVDF)-based membranes, and the pore sizes obtained were also smaller than those shown in

Figure 12 [33]. Recently, Nuaimi et al. also used the same material (PVDF) to obtain pore sizes between 3 and 100 nm [40].


Figure 12. Average pore size for each membrane. Note: M0 (no AC); M1 (PANREAC, 0.10%); M2 (PANREAC, 0.50%); M3 (Norit R, 0.10%); M4 (Norit R, 0.50%); M5 (Norit R, 1.00%); M6 (Norit R, 1.50%); M7 (Norit R, 2.00%); M8 (Norit PK, 0.10%); M9 (Norit PK, 0.50%). Grey bar: membrane without AC; Red bar: PANREAC AC membrane; Green bar: Norit R AC membrane; Blue bar: Norit PK membrane.

3.7. Field Emission Scanning Electron Microscopy Analysis

Field emission scanning electron microscopy (FESEM) analysis was carried out to visualise the synthesised membrane morphology. Figure 13 shows different perspectives of the pore structure observed for the no-AC membrane, as well as for the membranes doped with each of the studied ACs. A finger-like pore structure with the presence of certain macro-voids has been reported as the typical structure obtained in membranes synthesised by non-solvent-induced phase separation [36,39], and it is clearly observed in M0 (No AC membrane), corresponding to Figure 13a. PES membranes promote the formation of channels and more sponge-like structures [41]. Through the FESEM images, the membranes exhibited a structure with macro-holes and micro-holes. However, the effect of the addition of activated carbon generates a greater number of microholes, forming a spongy construction between fingers, as is observed in Figure 13b,d.

When focusing on the internal faces of membrane fingers, all the AC/PES membranes show a spongy substructure between the fingers. M2 shows a particularly close structure, with a relatively homogeneous distribution of fingers throughout its construction. This would explain the reduction in the passage of water and PEG molecules, mainly through narrow pores, increasing the rejection capacity due to these channels. The M4 image exhibits a disorganised finger structure and the closest pore distribution. While permeability presents a light reduction (compared to the reference membrane, M0, as seen in Table 2), a larger rejection is obtained. The opposite effect can be observed in the M9 membrane, where larger pores were developed, leading to a larger permeability and a drop in its rejection compared to the reference membrane.
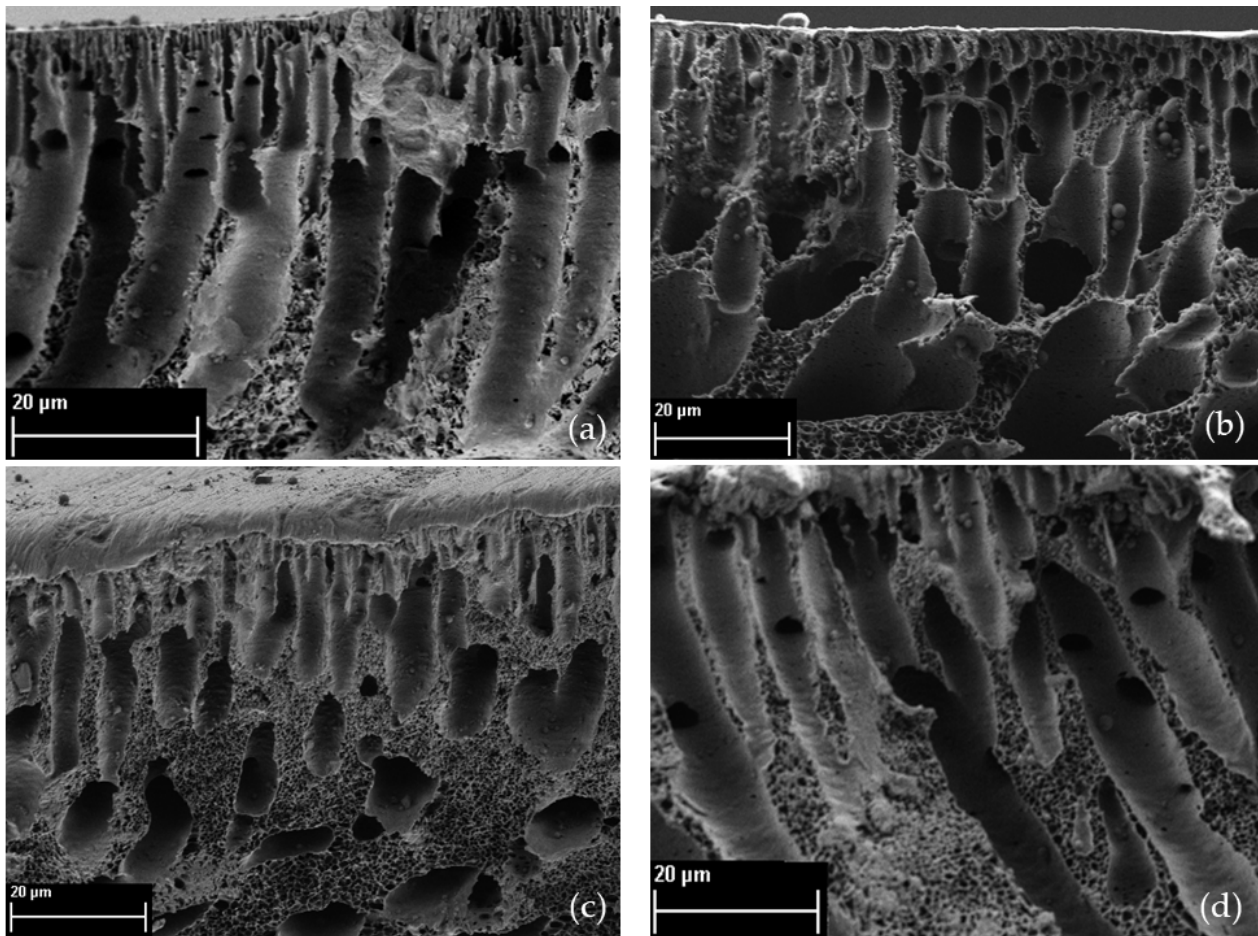
Figure 13. FESEM images of the membrane cross-sections of M0 (**a**), M2 (**b**), M4 (**c**), M9 (**d**). Note: M0 (no AC); M2 (PANREAC, 0.50%); M4 (Norit R, 0.50%); M9 (Norit PK, 0.50%).

4. Conclusions

This study has demonstrated the feasibility of producing hybrid membranes using activated carbons as dopants and the non-solvent-induced phase-inversion. In this work, we have demonstrated that these membranes can satisfactorily be manufactured and that the characterisation results obtained allowed us to gain insights into the membrane's characteristics, their performance, and the effect of the activated carbon properties on their behaviour. Of course, the optimum conditions and ideal activated carbon properties to achieve the best performance in the final hybrid membranes are still to be further investigated.

Regarding ACs' characterisation, both PANREAC and Norit PK showed the presence of a microporous configuration, while Norit R had a greater presence of mesoporosity. Nevertheless, these structures are considered suitable pore sizes for filtration and adsorption. Additionally, PANREAC AC was found to have the largest BET surface area of the ACs studied.

In respect of hybrid membranes, they were tested for their potential to remove contaminants from wastewater. Different ACs and loadings were introduced into the UF membrane structures and tested to determine their applicability and real limits. The PES-AC/DMA solution allowed us to obtain stable membranes using the NIPS method. AC loadings into the membranes of up to 2.0 wt. (%) were only achieved for Norit R activated carbon, whereas smaller loadings of 0.1 and 0.5 wt. (%) for the other two ACs studied could be added to obtain a homogeneous hybrid membrane. An increase in the spongy structure between the fingers was observed in all the PES/AC membranes, which provide an increase

in porosity and, therefore, in permeability. Additionally, for the M4 membrane (0.5 wt. (%) of Norit R added), an increase in the R index was observed, exhibiting a 80.34% rejection of PEG 35 kDa, being the optimal configuration for this series of doped membranes fabricated.

Additionally, it is essential to highlight that S_{BET}, L_0, and W_0 were the key textural properties of the three ACs that significantly influenced the rejection of the membrane to the studied compound. The addition of AC increased the hydrophilic characteristic of the membrane, generally producing low fouling rates. For membranes with smaller pores, the layer formed was simply rinsed away, and recovery rates ware high.

Future investigation in this field should introduce specific modifications in AC processing to obtain the ideal mesoporous structure that still allows us to maintain fluxes in membrane filtration and larger rejections. As sustainable alternatives are needed nowadays, a creative combination of existing techniques or resources like those explored in this work has great potential to lead to environmentally friendly solutions.

Author Contributions: Conceptualization, C.F.-M. and M.I.I.-C.; membrane investigation, R.M.-C. and A.I.-C.; activated carbon investigation, S.B.; data analysis, R.M.-C., S.B., A.I.-C. and E.M.G.-C.; writing—original draft preparation, R.M.-C. and S.B.; writing—review and editing, E.M.G.-C., C.F.-M. and M.I.I.-C.; supervision, E.M.G.-C., C.F.-M. and M.I.I.-C. All authors have read and agreed to the published version of the manuscript.

Institutional Review Board Statement: Not applicable.

Informed Consent Statement: Not applicable.

Data Availability Statement: No data was used for the research described in the article.

Conflicts of Interest: The authors declare no conflicts of interest.

Abbreviations

AC, activated carbon; BET, Brunauer–Emmet–Teller; COD, chemical oxygen demand; DFT, Density Functional Theory; DMA, dimethylacetanamide; DR, Dubinin–Radushkevich; DTG, derivative thermogravimetric curve; EWC, equilibrium water content; FESEM, field emission scanning electron microscopy; FRR, flux recovery ratio; MWCO, molecular weight cut-off; NIPS; non-solvent-induced phase separation; NOM, natural organic matter; PES, polyethersulfone; PEG, polyethylene glycol; PSD, Pore Size Distribution; PVDF, polyvinylidene fluoride; R, rejection index; SDGs, Sustainable Development Goals; TGA, Thermogravimetric Analyser; TMP, transmembrane pressure; UF, ultrafiltration.

References

1. Sustainable Development Goals. United Nations Publications. Available online: https://sdgs.un.org/publications (accessed on 20 December 2022).
2. Davidson, N.C. How much wetland has the world lost? Long-term and recent trends in global wetland area. *Mar. Freshwater Res.* **2014**, *65*, 934–941. [CrossRef]
3. Zhu, X.; Jin, L.; Yang, J.; Wu, J.; Zhang, B.; Zhang, X.; Yu, N.; Wei, S.; Wu, J.; Yu, H. Perfluoroalkyl acids in the water cycle from a freshwater river basin to coastal waters in eastern China. *Chemosphere* **2017**, *168*, 390–398. [CrossRef]
4. Kurwadkar, S.; Kanel, S.R.; Nakarmi, A. Groundwater pollution: Occurrence; detection, and remediation of organic and inorganic pollutants. *Water Environ. Res.* **2020**, *92*, 1659–1668. [CrossRef] [PubMed]
5. Bulatović, S.; Ilić, M.; Knudsen, T.Š.; Milić, J.; Pucarević, M.; Jovančićević, B.; Vrvić, M.M. Evaluation of potential human health risks from exposure to volatile organic compounds in contaminated urban groundwater in the Sava river aquifer, Belgrade, Serbia. *Environ. Geochem. Health* **2021**, *44*, 3451–3472. [CrossRef] [PubMed]

6. Howe, K.J.; Clark, M.M. Fouling of Microfiltration and Ultrafiltration Membranes by Natural Waters. *Environ. Sci. Technol.* **2002**, *36*, 3571–3576. [CrossRef] [PubMed]

7. Speth, T.F.; Summers, R.S.; Gusses, A.M. Nanofiltration Foulants from a Treated Surface Water. *Environ. Sci. Technol.* **1998**, *32*, 3612–3617. [CrossRef]

8. Al-Malack, M.H.; Anderson, G.K. Coagulation-crossflow microfiltration of domestic wastewater. *J. Membr. Sci.* **1996**, *121*, 59–70. [CrossRef]

9. Sonal, S.; Mishra, B.K. Role of Coagulation/Flocculation Technology for the Treatment of Dye Wastewater: Trend and Future Aspects. In *Water Pollution and Management Practices*; Singh, A., Agrawal, M., Agrawal, S.B., Eds.; Springer: Singapore, 2021; pp. 303–331. [CrossRef]

10. Chapman, H.; Vigneswaran, S.; Ngo, H.H.; Dyer, S.; Aim, R.B. Pre-flocculation of secondary treated wastewater in enhancing the performance of microfiltration. *Desalination* **2002**, *146*, 367–372. [CrossRef]

11. Amiri, Z.; Moussavi, G.; Mohammadi, S.; Giannakis, S. Development of a VUV-UVC/peroxymonosulfate, continuous-flow Advanced Oxidation Process for surface water disinfection and Natural Organic Matter elimination: Application and mechanistic aspects. *J. Hazard. Mater.* **2021**, *408*, 124634. [CrossRef] [PubMed]

12. Abdessemed, D.; Nezzal, G.; Aim, R.B. Coagulation-adsorption-ultrafiltration for wastewater treatment and reuse. *Water Supply* **2003**, *3*, 361–365. [CrossRef]

13. Mosbah, M.B.; Mechi, L.; Khiari, R.; Moussaoui, Y. Current State of Porous Carbon for Wastewater Treatment. *Processes* **2020**, *8*, 1651. [CrossRef]

14. Soffian, M.S.; Halim, F.Z.A.; Aziz, F.; Rahman, M.A.; Amin, M.A.M.; Chee, D.N.A. Carbon-based material derived from biomass waste for wastewater treatment. *Environ. Adv.* **2022**, *9*, 100259. [CrossRef]

15. Naddeo, V.; Secondes, M.F.N.; Borea, L.; Hasan, S.W.; Ballesteros, F.; Belgiorno, V. Removal of contaminants of emerging concern from real wastewater by an innovative hybrid membrane process—UltraSound, Adsorption, and Membrane ultrafiltration (USAMe®). *Ultrason. Sonochemistry* **2020**, *68*, 105237. [CrossRef] [PubMed]

16. Zhang, J.; Nguyen, M.N.; Li, Y.; Yang, C.; Schäfer, A.I. Steroid hormone micropollutant removal from water with activated carbon fiber-ultrafiltration composite membranes. *J. Hazard. Mater.* **2020**, *391*, 122020. [CrossRef] [PubMed]

17. Shao, S.; Cai, L.; Li, K.; Li, J.; Du, X.; Li, G.; Liang, H. Deposition of powdered activated carbon (PAC) on ultrafiltration (UF) membrane surface: Influencing factors and mechanisms. *J. Membr. Sci.* **2017**, *530*, 104–111. [CrossRef]

18. Liu, Q.; Huang, S.; Zhang, Y.; Zhao, S. Comparing the antifouling effects of activated carbon and TiO$_2$ in ultrafiltration membrane development. *J. Colloid Interface Sci.* **2018**, *515*, 109–118. [CrossRef] [PubMed]

19. Wolters, J.; Tagliavini, M.; Schäfer, A.I. Removal of steroid hormone micropollutants by UF-PBSAC composite in presence of organic matter. *J. Membr. Sci.* **2019**, *592*, 117315. [CrossRef]

20. Vicente, R.; Cesca, K.; da Silva, A.F.V.; de Oliveira, D.; de Andrade, C.J.; Ambrosi, A. Hierarchical membrane by centrifugal casting and effects of incorporating activated carbon as pore-former. *J. Eur. Ceram. Soc.* **2023**, *43*, 3447–3453. [CrossRef]

21. El-Sayed, M.Y.; Alsohaimi, I.H.; Alrashidi, A.N.; Aldawsari, A.M.; Alshahrani, A.A.; Hassan, H.M.A. Mixed matrix membrane comprising functionalized sulfonated activated carbon from tea waste biomass for enhanced hydrophilicity and antifouling properties. *Diam. Relat. Mater.* **2023**, *136*, 109945. [CrossRef]

22. Basko, A.; Lebedeva, T.; Yurov, M.; Ilyasova, A.; Elyashevich, G.; Lavrentyev, V.; Kalmykov, D.; Volkov, A.; Pochivalov, K. Mechanism of PVDF Membrane Formation by NIPS Revisited: Effect of Precipitation Bath Nature and Polymer–Solvent Affinity. *Polymers* **2023**, *15*, 4307. [CrossRef]

23. Singh, R. *Membrane Technology and Engineering for Water Purification*, 2nd ed.; Elsevier: Amsterdam, The Netherlands, 2015.

24. Lopatina, A.; Anugwom, I.; Blot, H.; Conde, Á.S.; Mänttäri, M.; Kallioinen, M. Re-use of waste cotton textile as an ultrafiltration membrane. *J. Environ. Chem. Eng.* **2021**, *9*, 105705. [CrossRef]

25. Fababuj-Roger, M.; Mendoza-Roca, J.A.; Galiana-Aleixandre, M.V.; Bes-Piá, A.; Cuartas-Uribe, B.; Iborra-Clar, A. Reuse of tannery wastewaters by combination of ultrafiltration and reverse osmosis after a conventional physical-chemical treatment. *Desalination* **2007**, *204*, 219–226. [CrossRef]

26. Ivars, J.G. Obtención Y Caracterización de Membranas Poliméricas de Ultrafiltración de Bajo Ensuciamiento Y Estudio de Condiciones de Fabricación. Doctoral Thesis, Universitat Politècnica de València, Valencia, Spain, 2015. [CrossRef]

27. Garcia-Ivars, J.; Wang-Xu, X.; Iborra-Clar, M.-I. Application of post-consumer recycled high-impact polystyrene in the preparation of phase-inversion membranes for low-pressure membrane processes. *Sep. Purif. Technol.* **2017**, *175*, 340–351. [CrossRef]

28. Manyà, J.J.; González, B.; Azuara, M.; Arner, G. Ultra-microporous adsorbents prepared from vine shoots-derived biochar with high CO$_2$ uptake and CO$_2$/N$_2$ selectivity. *Chem. Eng. J.* **2018**, *345*, 631–639. [CrossRef]

29. Martín, C.F.; Stöckel, E.; Clowes, R.; Adams, D.J.; Cooper, A.I.; Pis, J.J.; Rubiera, F.; Pevida, C. Hypercrosslinked organic polymer networks as potential adsorbents for pre-combustion CO$_2$ capture. *J. Mater. Chem.* **2011**, *21*, 5475–5483. [CrossRef]

30. Martín, C.F.; Plaza, M.G.; García, S.; Pis, J.J.; Rubiera, F.; Pevida, C. Microporous phenol–formaldehyde resin-based adsorbents for pre-combustion CO$_2$ capture. *Fuel* **2011**, *90*, 2064–2072. [CrossRef]

31. Baker, R.W. Membrane Transport Theory. In *Membrane Technology and Applications*; John Wiley & Sons, Ltd.: Hoboken, NJ, USA, 2004; pp. 15–87.

32. Mulder, M. *Basic Principles of Membrane Technology*; Springer: Dordrecht, The Netherlands, 1996. [CrossRef]

33. Wu, G.; Gan, S.; Cui, L.; Xu, Y. Preparation and characterization of PES/TiO$_2$ composite membranes. *Appl. Surf. Sci.* **2008**, *254*, 7080–7086. [CrossRef]

34. Bang, J.-H.; Lee, B.-H.; Choi, Y.-C.; Lee, H.-M.; Kim, B.-J. A Study on Superior Mesoporous Activated Carbons for Ultra Power Density Supercapacitor from Biomass Precursors. *Int. J. Mol. Sci.* **2022**, *23*, 8537. [CrossRef] [PubMed]

35. Sternik, D.; Wiśniewska, M.; Nowicki, P. Thermal degradation of peat-based activated carbons covered with mixed adsorption layers of PAA polymer and SDS surfactant. *Thermochim. Acta* **2019**, *676*, 71–83. [CrossRef]

36. Liu, S.; Chu, Y.; Tang, C.; He, S.; Wu, C. High-performance chlorinated polyvinyl chloride ultrafiltration membranes prepared by compound additives regulated non-solvent induced phase separation. *J. Membr. Sci.* **2020**, *612*, 118434. [CrossRef]

37. Cai, Y.; Schwartz, D.K. Single-nanoparticle tracking reveals mechanisms of membrane fouling. *J. Membr. Sci.* **2018**, *563*, 888–895. [CrossRef]

38. Mehrparvar, A.; Rahimpour, A.; Jahanshahi, M. Modified ultrafiltration membranes for humic acid removal. *J. Taiwan Inst. Chem. Eng.* **2014**, *45*, 275–282. [CrossRef]

39. Wang, H.H.; Jung, J.T.; Kim, J.F.; Kim, S.; Drioli, E.; Lee, Y.M. A novel green solvent alternative for polymeric membrane preparation via nonsolvent-induced phase separation (NIPS). *J. Membr. Sci.* **2019**, *574*, 44–54. [CrossRef]

40. Nuaimi, R.A.; Thankamony, R.L.; Liu, X.; Cao, L.; Zhou, Z.; Lai, Z. Ultrafiltration membranes prepared via mixed solvent phase separation with enhanced performance for produced water treatment. *J. Membr. Sci.* **2023**, *670*, 121375. [CrossRef]

41. Barzin, J.; Sadatnia, B. Correlation between macrovoid formation and the ternary phase diagram for polyethersulfone membranes prepared from two nearly similar solvents. *J. Membr. Sci.* **2008**, *325*, 92–97. [CrossRef]